Yokohama Publishers
ISSN 1349-8169 ONLINE JOURNAL

Pacific Journal of Optimization
Vol. 21, No. 3, pp. 413–430, 2025

PENALTY APPROACHES FOR LOW-ORDER FILTER DESIGN IN SOUND FIELD CONTROL

Shu Tan, Hao Luo, Xiangning Liao, Fusheng Bai* and Jie Li

Abstract: Sound field control is widely used in various scenarios to create distinct acoustic environments within specific zones. Two novel low-order filter design methods for sound field control have been proposed by integrating finite difference penalties of L1-norm and L2-norm with the ACC-PM method. This approach enables the generation of low-order time-domain filters for the loudspeaker array, while accurately reproducing the target amplitude and phase distribution in a specific sound field. The alternating direction method of multipliers (ADMM) algorithm is employed to solve the proposed models. Numerical experimental results demonstrate that, compared to four benchmark sound field control methods, the two proposed methods can effectively reduce the filter order.

Key words: *sound field control, personal audio system, low-order time-domain filter, finite difference penalty*

Mathematics Subject Classification: *90C25, 90C90*

1 Introduction

Sound field control involves using multiple loudspeakers to create distinct acoustic environments within specific zones [5, 7, 8, 10, 20] and has numerous applications in various scenarios, including automotive cabins, museums, and more [6, 15]. In this process, filters play a pivotal role by providing precise control over the amplitude and phase of broadband frequency driving signals of loudspeakers. By utilizing filters to adjust the sound characteristics in each field zone, it is possible to create acoustically bright and dark zones and effectively reproduce target sound fields [6, 9].

In practical applications, we utilize single-input multiple-output (SIMO) finite impulse response (FIR) filters [15] to generate the driving signals for the loudspeaker array. These time-domain signals are played through the loudspeakers to synthesize the desired sound field in a specified area, thereby achieving sound field control. The coefficients of the filters are determined using sound field partitioning control methods. These coefficients are the weight signals of the loudspeaker array in the frequency domain, obtained through an inverse Fourier transform.

The order of a filter is intricately tied to the oscillation level of the frequency sound signal [1, 20]. In general, higher oscillation level corresponds to higher order. This association arises

*Corresponding author. The work of Fusheng Bai was supported in part by the National Key R&D Program of China under Project 2023YFA1011802 and the Innovation and Development Joint Program of the Chongqing Natural Science Foundation under Project CSTB2022NSCQ-LZX0012.

 DOI: https:// doi.org/10.61208/pjo-2025-020

from the necessity for a higher filter order to effectively capture and process the intricate oscillatory components in the frequency-domain driving signal. However, a higher order implies higher filter manufacturing costs and increased time delay. Consequently, when designing filters for sound field control, it becomes imperative to reduce the oscillation level at lower frequencies, thereby mitigating the need for an unnecessarily high-order filter.

Sound field control methods fall into two categories: Sound Field Synthesis [21] and Beamforming. The former exemplified by Pressure Matching (PM), focuses on accurately synthesizing a specified sound field. In contrast, Beamforming, represented by Acoustic Contrast Control (ACC), directs a beam towards a specific direction, enhancing perceptual contrast. Comparative studies reveal that ACC provides maximum acoustic contrast across frequencies but exhibits poor accuracy in sound field synthesis and inadequate lower-frequency gain [8, 18]. Conversely, PM demonstrates superior accuracy in sound field synthesis and satisfactory contrast but demands consistently high control effort [8]. To address this, the ACC-PM method has been introduced, offering flexibility in adjusting hyper-parameters for a balanced trade-off between the accuracy of bright zone synthesis and the acoustic contrast [5]. This method provides a more adaptable approach to acoustic field control.

In earlier research, various approaches aimed at constraining the driving signal to minimize oscillation levels have been explored. One such method is the ACC-multi-point equalization method [2, 3], which adjusts the driving signals computed by the ACC in both amplitude and phase to lower oscillation levels. This method not only effectively shortens the filter order but also improves contrast at non-control frequency points compared to using ACC alone. Another study introduces a L2-norm based finite difference penalty term to Amplitude Matching (AM), a sound field synthesis method [1], effectively reducing the oscillation level of the driving signal, particularly the phase oscillation level. The AM method only reproduces the target amplitude, while the phase distribution remains arbitrary.

The application of L2-norm penalty term as a regularization technique is crucial for providing stability to various methods. In the intricate domain of sound field control, regularization is essential for reducing numerical errors and improving the condition number during matrix inversion [6]. This not only enhances continuity in modal control but also provides a clear physical definition for the involved processes [11]. Beyond the scope of the L2-norm penalty term, the L1-norm penalty term is equally influential and is well-known for its ability to induce sparsity. This property has made it widely applicable in various signal processing tasks. Its versatility extends to promoting signal sparsity, facilitating feature selection, executing denoising procedures, and enabling sparse representation, among other tasks [17, 19]. This broad range of uses highlights the significance and adaptability of the L1-norm penalty term in signal processing.

In this paper, the utilization of the finite difference penalty in the ACC-PM method (ACC-PM-L2) is implemented to synthesize the desired amplitude and phase while simultaneously reducing the oscillation level of the driving signal. Moreover, a finite difference penalty term based on the L1-norm (Diff.-L1 penalty) is introduced in ACC-PM (ACC-PM-L1) to improve the flatness of the driving signal by enhancing the sparsity of the difference penalty, thereby reducing the order of the filters. The incorporation of the L1-norm penalty is considered a form of feature extraction on the broadband driving signals. This process not only preserves their primary characteristics but also compresses the informational content embedded in the signals [4]. Due to the nature of the ACC-PM-L1 cost function, the Alternating Direction Method of Multipliers (ADMM) is selected for rapidly solving the optimization problem [12].

The two methods proposed in this paper consistently exhibit superior characteristics in sound field control and filter order reduction. Users have the flexibility to fine-tune

parameters based on their specific sound field control requirements. Compared to other conventional sound field control methods, the filter order generated by our proposed methods is reduced by at least half.

The remaining sections of this paper are organized as follows: Section 2 provides preliminaries. In Section 3, two models have been established, utilizing low-order filters to control sound field using the ACC-PM method combined with two difference penalties. An efficient algorithm to solve these models is presented using the ADMM method. In Section 4, experiments conducted in a free field scenario are presented.

2 Preliminaries

This section provides a brief introduction to the sound field control system and reviews some existing well-known methods.

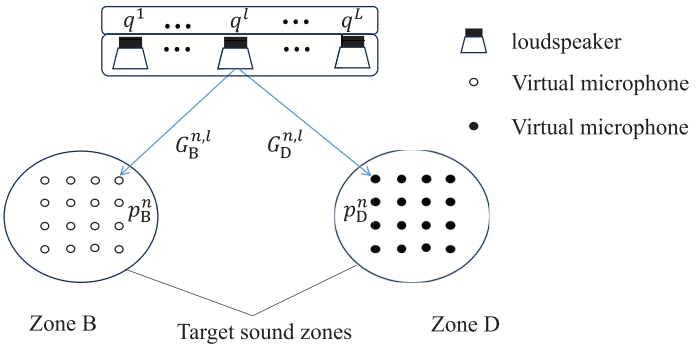

Figure 1: Illustration of a personal sound control system.

Below in Figure 1, we illustrate a conventional loudspeaker array-based sound field control system, which consists of L loudspeakers and two sound zones, denoted as B and D. In each sound zone, there are several virtual microphones that serve as control points.The goal is to determine the optimal driving signals for the loudspeaker array using sound field partitioning control methods, thereby synthesizing the desired sound field within the sound zones $\Omega \in \{\mathrm{B}, \mathrm{D}\}$.

Integrating Figure 1, we introduce the fundamental acoustic principles of sound field partitioning control. For each angular frequency f, the input driving signal vector of the loudspeaker array is $\mathbf{q}(f) = [q^1(f), q^2(f), ..., q^L(f)]^T \in \mathbb{C}^L$. It is worth noting that angular frequencies are omitted in Figure 1 for the sake of simplicity. Assume there are N_Ω control points in the zone Ω. Let $G_\Omega^{n,l}(f)$ be the acoustic transfer function between the n-th control microphone in Ω and the l-th loudspeaker. Then the sound pressure at the n-th control point is expressed as

$$p_\Omega^n(f) = \sum_{l=1}^{L} G_\Omega^{n,l} q^l, \quad n = 1, 2, \cdots, N_\Omega. \tag{2.1}$$

This allows a more compact matrix-vector form

$$\mathbf{p}_\Omega(f) = \boldsymbol{G}_\Omega(f)\mathbf{q}(f), \quad \Omega \in \{\mathrm{B}, \mathrm{D}\}, \tag{2.2}$$

where $\mathbf{p}_\Omega(f) = [p_\Omega^1(f), p_\Omega^2(f), \cdots, p_\Omega^{N_\Omega}(f)]^T \in \mathbb{C}^{N_\Omega}$ represents the sound pressure vector in the zone Ω , and the transfer function matrix is given by

$$\boldsymbol{G}_\Omega(f) = \begin{bmatrix} G_\Omega^{1,1}(f) & \cdots & G_\Omega^{1,L}(f) \\ \vdots & \ddots & \vdots \\ G_\Omega^{N_\Omega,1}(f) & \cdots & G_\Omega^{N_\Omega,L}(f) \end{bmatrix}.$$

Based on the acoustic principles described above, we will now provide a brief introduction to the three commonly used sound field partitioning control methods.

2.1 Acousic contrast control (ACC)

Acoustic Contrast Control (ACC) [7, 8] is a beamforming-based method of sound field control that aims to generate acoustic bright and dark zones. The optimization problem of ACC is defined as maximizing the acoustic contrast between the bright and dark zones as follows:

$$\max_{\mathbf{q}(f)\in\mathbb{C}^L} J(\mathbf{q}(f)) := \frac{N_\mathrm{D}}{N_\mathrm{B}} \times \frac{\|\mathbf{p}_\mathrm{B}(f)\|^2}{\|\mathbf{p}_\mathrm{D}(f)\|^2} = \frac{N_\mathrm{D}}{N_\mathrm{B}} \times \frac{\|\boldsymbol{G}_\mathrm{B}(f)\mathbf{q}(f)\|^2}{\|\boldsymbol{G}_\mathrm{D}(f)\mathbf{q}(f)\|^2}, \tag{2.3}$$

where $\mathbf{p}_\mathrm{B}(f)$ and $\mathbf{p}_\mathrm{D}(f)$ are the reproducing pressures of the bright and dark zones respectively, while $\mathbf{G}_\mathrm{B}(f)$ and $\mathbf{G}_\mathrm{D}(f)$ are the transfer function matrices of the bright and dark zones respectively. The maximization Equation (2.3) equates to the generalized eigenvalue problem

$$\boldsymbol{G}_\mathrm{B}(f)^H\boldsymbol{G}_\mathrm{B}(f)\mathbf{q}(f) = \lambda[\boldsymbol{G}_\mathrm{D}^H(f)\boldsymbol{G}_\mathrm{D}(f) + \mu\boldsymbol{I}]\mathbf{q}(f),$$

where $\lambda \in \mathbb{R}$ is the largest eigenvalue, μ is the regularization parameter, and the optimal solution $\mathbf{q}^\star(f)$ to Equation (2.3) is an eigenvector of λ.

2.2 Amplitude matching (AM)

Amplitude matching (AM) [1] only concerns reproducing amplitude of the sound field, and the phase is arbitrary. The optimization problem of amplitude matching is as follows:

$$\min_{\mathbf{q}(f)\in\mathbb{C}^L} \left\| |\mathbf{p}(f)| - |\mathbf{p}_\mathrm{T}(f)| \right\|^2 = \left\| |\boldsymbol{G}(f)\mathbf{q}(f)| - |\mathbf{p}_\mathrm{T}(f)| \right\|^2, \tag{2.4}$$

where $\mathbf{p}(f)$ is the reproducing pressure and $\mathbf{p}_\mathrm{T}(f)$ is the target pressure.

2.3 Pressure matching (PM)

Pressure Matching (PM) [21] is a sound field synthesis method aimed at reproducing the desired acoustic field. The optimization problem of PM can be defined as minimizing the error in bright zone and the energy in dark zone as follows:

$$\min_{\mathbf{q}(f)\in\mathbb{C}^L} \|\mathbf{p}_\mathrm{B}(f) - \mathbf{p}_{\mathrm{BT}}(f)\|^2 + \delta \|\mathbf{p}_\mathrm{D}(f)\|^2 + \gamma \|q(f)\|^2, \tag{2.5}$$

where $\mathbf{p}_{\mathrm{BT}}(f) = [p_{\mathrm{BT}}^1(f), p_{\mathrm{BT}}^2(f), \cdots, p_{\mathrm{BT}}^{N_\mathrm{B}}(f)]^T \in \mathbb{C}^{N_\mathrm{B}}$ is the target pressure that needs to be reproduced in the bright zone, while $\delta > 0$ denotes the weight parameter and γ is the regularization parameter. The first term represents the sum of reproduction errors of the sound field in the bright zone at each control frequency point. The second term represents the total sound energy in the dark zone at each control frequency point, while the third term

is a regularization term designed to prevent the energy of the signal $\mathbf{q}(f)$ from becoming excessively large. Different weighting parameters represent different preferences for sound field zoning control. When $\delta = 1$, it amounts to the method of pressure matching (PM). In cases where the weight parameter δ can be arbitrarily specified, this method is known as ACC-PM [5]. Users can fine-tune the parameters according to their specific sound field control requirements to better balance the sound field partitioning control effects.

3 Finite difference penalty for low-order time-domain filter design

The utilization of low-order time-domain filters in sound field control offers an opportunity to reduce industrial manufacturing expenses while concurrently enhancing the stability of control system and reducing the system latency. Expanding upon the original ACC-PM method Equation (2.5), we introduce two novel methods incorporating finite difference penalty terms. The first method involves the L1-norm of the differences which promotes sparsity in the solution and reduces the signal complexity, while the second method involves the L2-norm of the differences to achieve smoother solutions. Both methods, based on the ACC-PM method, aim to flatten the frequency domain weight signal of the loudspeaker array.

3.1 ACC-PM with L2-norm based difference penalty

Note that the problem Equation (2.5) involves a fixed angular frequency. For the sake of presentation, assume there are J frequency points, denoted as $f_1, \cdots, f_J$. Introduce the overall driving signal and sound pressure as follows

$$\begin{aligned}\mathbf{q} &= [\mathbf{q}(f_1)^T, \cdots, \mathbf{q}(f_J)^T]^T \in \mathbb{C}^{JL},\\ \mathbf{p}_{\mathrm{BT}} &= [\mathbf{p}_{\mathrm{BT}}(f_1)^T, \cdots, \mathbf{p}_{\mathrm{BT}}(f_J)^T]^T \in \mathbb{C}^{JL}.\end{aligned}$$

Then we update Equation (2.5) to a broadband form across the frequency domain:

$$\min_{\mathbf{q}\in\mathbb{C}^{JL}} \left\|\boldsymbol{G}_{\mathrm{B}}\mathbf{q} - \mathbf{p}_{\mathrm{BT}}\right\|^2 + \delta \left\|\boldsymbol{G}_{\mathrm{D}}\mathbf{q}\right\|^2, \tag{3.1}$$

where $\boldsymbol{G}_\Omega = \mathrm{diag}\{\boldsymbol{G}_\Omega(f_1), \cdots, \boldsymbol{G}_\Omega(f_J)\}$ is a block diagonal matrix. It is straightforward to obtain the optimal closed-form solution:

$$\mathbf{q}^\star = (\boldsymbol{G}_{\mathrm{B}}^H\boldsymbol{G}_{\mathrm{B}} + \delta\boldsymbol{G}_{\mathrm{D}}^H\boldsymbol{G}_{\mathrm{D}})^{-1}\boldsymbol{G}_{\mathrm{B}}^H\mathbf{p}_{\mathrm{BT}}. \tag{3.2}$$

Recall that $\mathbf{q}(f_j) = [q^1(f_j), q^2(f_j), ..., q^L(f_j)]^T \in \mathbb{C}^L$ denotes the input driving signal vector of the loudspeaker array. To decrease the filter order over the time-domain, an indirect way is to improve the smoothness of the input signal of the loudspeaker. Specifically, the objective is to minimize the following quantities

$$\sum_{j=1}^{J-1} \left\|q^i(f_{j+1}) - q^i(f_j)\right\|^2, \quad i = 1, \cdots, L. \tag{3.3}$$

Plugging this penalty term into Equation (3.1) leads to

$$\min_{\mathbf{q}\in\mathbb{C}^{JL}} \left\|\boldsymbol{G}_{\mathrm{B}}\mathbf{q} - \mathbf{p}_{\mathrm{BT}}\right\|^2 + \delta_1 \left\|\boldsymbol{G}_{\mathrm{D}}\mathbf{q}\right\|^2 + \delta_2 \left\|\boldsymbol{F}\mathbf{q}\right\|^2, \tag{ACC-PM-L2}$$

where $\delta_1, \delta_2 > 0$ are weight parameters and $\boldsymbol{F} = \boldsymbol{D} \otimes \boldsymbol{I}_L$ where $\boldsymbol{D} \in \mathbb{R}^{(J-1)\times J}$ is a difference matrix that satisfies

$$D_{ij} = \begin{cases} -1, & \text{if } i = j, \\ 1, & \text{if } i = j-1, \\ 0, & \text{else.} \end{cases}$$

Analogously to Equation (3.1), the solution to problem Equation (ACC-PM-L2) is given by

$$\mathbf{q}^\star = (\boldsymbol{G}_{\mathrm{B}}^H \boldsymbol{G}_{\mathrm{B}} + \delta_1 \boldsymbol{G}_{\mathrm{D}}^H \boldsymbol{G}_{\mathrm{D}} + \delta_2 \boldsymbol{F}^H \boldsymbol{F})^{-1} \boldsymbol{G}_{\mathrm{B}}^H \mathbf{p}_{\mathrm{BT}}. \tag{3.4}$$

3.2 ACC-PM with L1-norm based difference penalty

Inspired by the l_1-norm for ensuring sparsity [19], we are also interested in the nonsmooth penalty

$$\sum_{j=1}^{J-1} \left\| q^i(f_{j+1}) - q^i(f_j) \right\|_1, \quad i = 1, \cdots, L, \tag{3.5}$$

where for any complex number or vector $\mathbf{z}$, $\|\mathbf{z}\|_1 := \|\mathrm{Re}(\mathbf{z})\|_1 + \|\mathrm{Im}(\mathbf{z})\|_1$. Consider the following model

$$\min_{\mathbf{q}\in\mathbb{C}^{JL}} \|\boldsymbol{G}_{\mathrm{B}}\mathbf{q} - \mathbf{p}_{\mathrm{BT}}\|^2 + \delta_1 \|\boldsymbol{G}_{\mathrm{D}}\mathbf{q}\|^2 + \delta_2 \|\boldsymbol{F}\mathbf{q}\|_1 . \tag{ACC-PM-L1}$$

Note that the l_1-norm seeks some signal vector $\mathbf{q}^*$ such that $\boldsymbol{F}\mathbf{q}^*$ is sparse while the use of l_2-norm aims for $\boldsymbol{F}\mathbf{q}^*$ to be small. Both two penalties strive to make the signal vector of each loudspeaker as flat as possible.

The objective function of this model Equation (ACC-PM-L1) is nonsmooth and lacks a closed-form solution, thus requiring numerical algorithms for solution. Given that it is a separable convex optimization problem in the complex domain of real-valued functions, it is suitable for ADMM. Moreover, each subproblem generated by ADMM has an analytical solution, significantly enhancing computational efficiency. Additionally, research has demonstrated the convergence of ADMM for solving such problems, noting its sublinear convergence rate $O(1/k)$ [14, 16].

Introduce a new variable $\mathbf{z} = \boldsymbol{F}\mathbf{q}$ and the augmented Lagrangian accordingly

$$\begin{aligned} \mathcal{L}_\rho(\mathbf{q}, \mathbf{z}; \boldsymbol{\mu}) = {} & \|\boldsymbol{G}_{\mathrm{B}}\mathbf{q} - \mathbf{p}_{\mathrm{BT}}\|^2 + \delta_1 \|\boldsymbol{G}_{\mathrm{D}}\mathbf{q}\|^2 + \delta_2 \|\mathbf{z}\|_1 \\ & + \mathrm{Re}(\boldsymbol{\mu}^H(\boldsymbol{F}\mathbf{q} - \mathbf{z})) + \frac{\rho}{2}\|\boldsymbol{F}\mathbf{q} - \mathbf{z}\|^2, \end{aligned}$$

where $\boldsymbol{\mu} \in \mathbb{C}^{(J-1)L}$ denotes the Lagrange multiplier and $\rho > 0$ is the penalty parameter. The standard ADMM [12] applies alternating minimization approach to $\mathcal{L}_\rho$ and is formulated as follows

$$\begin{cases} \mathbf{q}^{k+1} = \underset{\mathbf{q}\in\mathbb{C}^{JL}}{\operatorname{argmin}} \mathcal{L}_\rho(\mathbf{q}, \mathbf{z}^k; \boldsymbol{\mu}^k), \\ \mathbf{z}^{k+1} = \underset{\mathbf{z}\in\mathbb{C}^{(J-1)L}}{\operatorname{argmin}} \mathcal{L}_\rho(\mathbf{q}^{k+1}, \mathbf{z}; \boldsymbol{\mu}^k), \\ \boldsymbol{\mu}^{k+1} = \boldsymbol{\mu}^k + \tau\rho(\boldsymbol{F}\mathbf{q}^{k+1} - \mathbf{z}^{k+1}), \end{cases} \tag{3.6}$$

where $\tau \in (0, 2)$ is the step size and the initial guess is $(\mathbf{q}^0, \mathbf{z}^0, \boldsymbol{\mu}^0)$. After some calculations, the updating formulae of $\mathbf{q}^{k+1}$ and $\mathbf{z}^{k+1}$ are

$$\begin{cases} \mathbf{q}^{k+1} = (\boldsymbol{G}_{\mathrm{B}}^H \boldsymbol{G}_{\mathrm{B}} + \delta_1 \boldsymbol{G}_{\mathrm{D}}^H \boldsymbol{G}_{\mathrm{D}} + \delta_2 \boldsymbol{F}^H \boldsymbol{F})^{-1} \left(\boldsymbol{G}_{\mathrm{B}}^H \mathbf{p}_{\mathrm{BT}} + \frac{\rho}{2} \boldsymbol{F}^H \mathbf{z}^k - \frac{1}{2} \boldsymbol{F}^H \boldsymbol{\mu}^k \right), \\ \mathbf{z}^{k+1} = \mathbf{prox}_{t\|\cdot\|_1}(\boldsymbol{F}q^{k+1} + \boldsymbol{\mu}^k/\rho), \quad t = \delta_2/\rho, \end{cases} \tag{3.7}$$

where $\mathbf{prox}_{t\|\cdot\|_1}$ denotes the complex-valued soft shrinkage operator

$$\mathbf{prox}_{t\|\cdot\|_1}(\mathbf{z}) = \mathbf{prox}_{t\|\cdot\|_1}(\mathrm{Re}(\mathbf{z})) + i\,\mathbf{prox}_{t\|\cdot\|_1}(\mathrm{Im}(\mathbf{z})), \quad \mathbf{z} \in \mathbb{C}.$$

The overall ADMM iteration is summarized in Algorithm 1. For completeness, we provide some essential derivation details of Equation (3.7) in Appendix A.2.

Algorithm 1 ADMM for solving Equation (ACC-PM-L1)

Input: $\rho > 0$, $0 < \tau < 2$
Initialize $\mathbf{q}^0 \in \mathbb{C}^{JL}$, $\mathbf{z}^0, \boldsymbol{\mu}^0 \in \mathbb{C}^{(J-1)L}$
$\boldsymbol{A} = (\boldsymbol{G}_{\mathrm{B}}^H \boldsymbol{G}_{\mathrm{B}} + \delta_1 \boldsymbol{G}_{\mathrm{D}}^H \boldsymbol{G}_{\mathrm{D}} + \delta_2 \boldsymbol{F}^H \boldsymbol{F})$
for $k = 0, 1, \ldots$ **do**
  $\mathbf{q}^{k+1} = \boldsymbol{A}^{-1}(\boldsymbol{G}_{\mathrm{B}}^H + \frac{\rho}{2}\boldsymbol{F}^H \mathbf{z}^k - \frac{1}{2}\boldsymbol{F}^H \boldsymbol{\mu}^k)$
  $\mathbf{z}^{k+1} = \mathrm{prox}_{t\|\cdot\|_1}(\boldsymbol{F}\mathbf{q}^{k+1} + \boldsymbol{\mu}^k/\rho)$, $t = \delta_2/\rho$
  $\boldsymbol{\mu}^{k+1} = \boldsymbol{\mu}^k + \tau\rho(\boldsymbol{F}\mathbf{q}^{k+1} - \mathbf{z}^{k+1})$
  $err = \|\mathbf{q}^{k+1} - \mathbf{q}^k\| + \|\mathbf{z}^{k+1} - \mathbf{z}^k\| + \|\boldsymbol{\mu}^{k+1} - \boldsymbol{\mu}^k\|$
  if $err < \epsilon$ **then**
    break
  end if
end for
Output: Optimal solutions: $\mathbf{q}^* = \mathbf{q}^{k+1}$, $\mathbf{z}^* = \mathbf{z}^{k+1}$, $\boldsymbol{\mu}^* = \boldsymbol{\mu}^{k+1}$

4 Numerical experiments

We have conducted experiments to evaluate our proposed methods. Firstly, we have validated the effectiveness of Equations (ACC-PM-L2) and (ACC-PM-L1) using simulated data. Subsequently, we have tested the methods using real measured data, further confirming the efficacy of the methods in practical applications.

4.1 Metrics for performance measurement

Let us introduce three key metrics for measuring the quality of the signal $\mathbf{q}$. One is the percentage of normalized mean-square error between reproduced and target sound field in the bright zone

$$E_r(f) := \frac{\|\mathbf{p}_{\mathrm{B}}(f) - \mathbf{p}_{\mathrm{BT}}(f)\|^2}{\|\mathbf{p}_{\mathrm{BT}}(f)\|^2},$$

which involves the ratio of the mean sum of the square error in the bright sound zone between reproducing pressure $p_{\mathrm{B}}(f)$ and target pressure $p_{\mathrm{BT}}(f)$ to target pressure $p_{\mathrm{BT}}(f)$.

The second is the acoustic contrast

$$AC(f) := 10\log_{10}\frac{N_{\mathrm{D}}}{N_{\mathrm{B}}} \times \frac{\|\mathbf{p}_{\mathrm{B}}(f)\|^2}{\|\mathbf{p}_{\mathrm{D}}(f)\|^2},$$

which is the ratio of the average sound energy density in the bright zone to that in the dark zone. It evaluates the effectiveness of the distinction between the bright and dark zones.

The other one is the center energy percentage in the pre-truncated filter, which involves the inverse FFT of $\mathbf{q}$. More precisely, let $\triangle f$ be the interval between control frequency points and f_s the sampling frequency. The inverse FFT of $\mathbf{q}$ is denoted by $\mathbf{w} = (w(0), ..., w(I)) \in \mathbb{R}^I$, with $I = f_s/\triangle f$. For given $K \in \mathbb{N}$, the center energy percentage is define by

$$E_c(K) := \frac{1}{\|\mathbf{w}\|^2} \sum_{i=\frac{I}{2}-\frac{K}{2}}^{\frac{I}{2}+\frac{K}{2}} w(i)^2,$$

which stands for the proportion of total energy before truncation to the energy within the central order.

With the metric $E_c(K)$, we can determine the order and coefficients of the filter. Due to the possibility of low-amplitude coefficients at both ends before truncation, a common practice is to truncate only the central part containing larger numerical values. This reduces computational and storage costs while preserving the main characteristics of the filter. Typically, we truncate the central part to retain 99% of the total energy, determining the filter order K as follows:

$$K = \min\{K : C(K) \geq 0.99, K \in \mathbb{N}\}.$$

It is noteworthy that once the optimal solution $\mathbf{q}^*$ for the speaker array weight signals is determined, the corresponding filter order K and filter coefficients are also determined. The filter coefficients are given by $[F(I/2 - K/2), \ldots, F(I/2 + K/2)]$.

4.2 Experiment results

We have conducted numerical experiments through 3D free field simulations. A real car with dimensions of approximately

$$\text{length} \times \text{width} \times \text{height} = 3m \times 1.8m \times 1.3m$$

is approximately denoted by a rectangular prism, as depicted in Figure 2. The orange and red blocks in Figure 2 represent the ear areas of the front-row and rear-row passengers inside the car. The positioning of the speaker array on the car roof is illustrated in Figure 3.

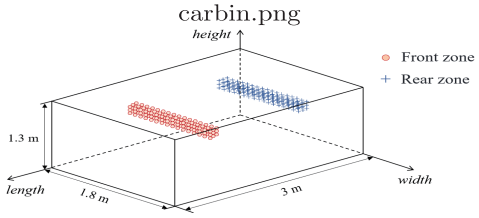

Figure 2: Simplified car model.

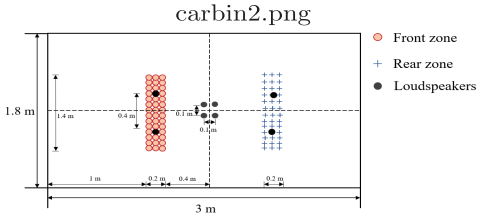

Figure 3: Loudspeakers position.

In our framework, we designate the front row as the bright zone Ω_B and the rear row as the dark zone Ω_D. For the target sound pressure, we set it to 1.0 in Ω_B and 0.0 in Ω_D. The generated signal is a band-limited pulse signal ranging from 200 Hz to 1200 Hz. The interval between control frequency points $\triangle f$ is set to 1, and the sampling frequency is 48 kHz, consistent with the number of frequency bins. The transfer function matrix is simulated and generated based on acoustic principles, as detailed in reference [15].

To validate the performance of the sound field control methods proposed in this paper, Equations (ACC-PM-L1) and (ACC-PM-L2), we compare them with four existing methods: ACC, PM, ACC-PM, and AM with smooth difference penalty (AM-L2). The model for AM-L2 is as follows:

$$\min_{\mathbf{q}(f)\in\mathbb{C}^L} F(\mathbf{q}(f)) := \| |\boldsymbol{G}(f)\mathbf{q}(f)| - |\mathbf{p}_{\mathrm{T}}(f)| \|^2 + \rho \|\boldsymbol{F}\mathbf{q}\|^2, \tag{4.1}$$

The regularization parameter μ in Equation (2.3) for ACC and γ in Equation (2.5) for PM are both set as 1.0×10^{-5}. The penalty parameter in Equation (4.1) for AM-L2 is set to 10. The parameter δ_1 and δ_2 are set to 8.3 and 24 in both Equation (ACC-PM-L1) and

Equation (ACC-PM-L2). Meanwhile, in the control group ACC-PM, parameter δ is set as 8.3. Once this parameters are determined, the optimal driving signals for the loudspeaker-array in the frequency domain can be obtained by using the sound field control methods. Transforming these signals into the time domain yields the corresponding filters. Figure 5 provides a schematic diagram of the untruncated filters.

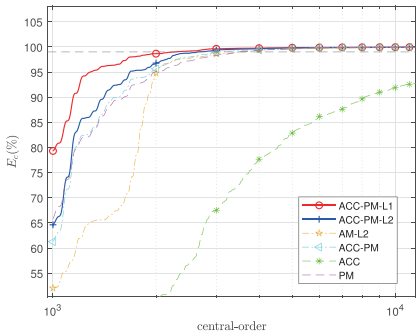

Figure 4: The trend of E_c with respect to the central order.

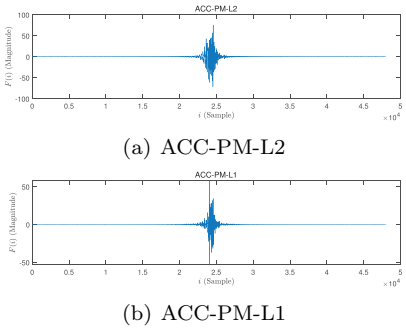

(a) ACC-PM-L2

(b) ACC-PM-L1

Figure 5: The 4th loudspeaker filters generated by methods.

Observing Figure 5, it becomes evident that the ACC-PM-L1 method exhibits the most pronounced truncation effect, with a notable concentration of energy in the filter points. Figure 4 illustrates the trend of E_c with respect to the central order. The optimal filter order K is defined as the central order such that $E_c(K)$ is 99%.

As indicated in Table 1, the ACC-PM-L1 method has the lowest average filter order 1952, followed by the ACC-PM-L2 method, which is 2226.

Table 1: The optimal filters order

	The optimal order of the 4th filter	The average optimal order of all filters
ACC-PM-L1	2272	1952
ACC-PM-L2	2560	2226
AM-L2	3612	2763
ACC-PM	3056	2919
ACC	38650	36576
PM	3516	3313

From Figure 6, it can be observed that compared to ACC-PM, the two methods proposed in this paper yield smoother amplitude and phase curves with respect to frequency due to the inclusion of penalty terms. The other methods exhibit characteristics in the frequency domain according to their distinct properties, reflected in their corresponding amplitude and phase curves. Furthermore, the introduction of the L1 penalty, as opposed to the L2 penalty, has exhibited sparsity, preserving valuable information while proving more effective in reducing the oscillation level of the signal.

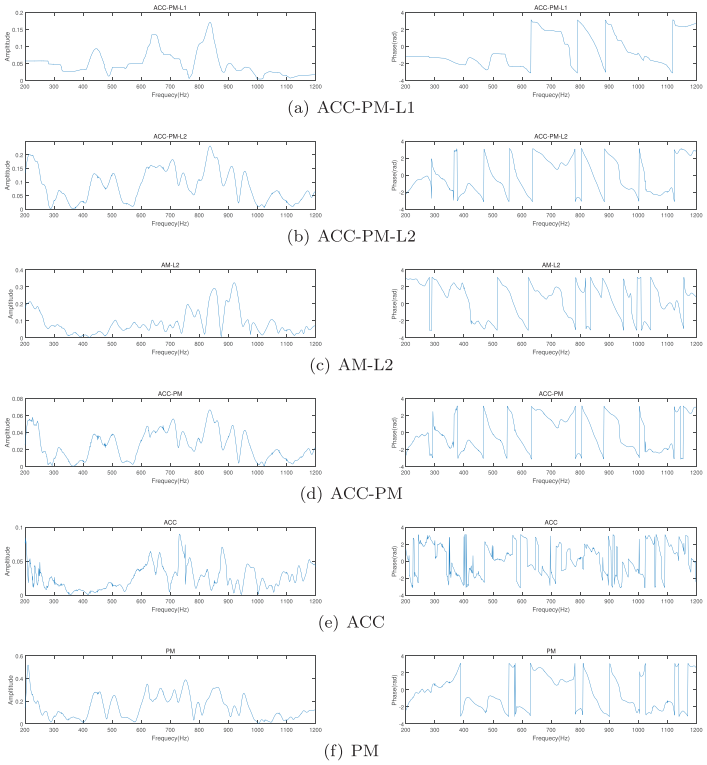

Figure 6: The 4th loudspeaker driving signal amplitude and phase.

Table 2: The average E_r and AC for all the frequency bins

	ACC-PM-L1	ACC-PM-L2	AM-L2	ACC-PM	ACC	PM
$\bar{E_r}$	0.06	0.035	1.12	0.29	0.81	0.02
$\bar{AC}$	23.87	27.16	27.13	27.39	50.11	21.80

The average E_r and AC are defined for all the frequency bins as

$$\bar{E_r} = \frac{1}{J}\sum_{i=1}^{J} E_r(f_i), \quad \bar{AC} = \frac{1}{J}\sum_{i=1}^{J} AC(f_i). \tag{4.2}$$

Figure 7 presents a comparison of the proposed methods with ACC and PM in terms of the metrics AC and E_r, demonstrating the effectiveness of the two methods in achieving sound field partitioning control. Figure 8 compares the proposed methods, ACC-PM and AM-L2. Compared to ACC-PM, the penalty terms significantly reduce the reproduction error in the bright zone sound field. Compared to AM-L2, the proposed methods show superior accuracy in sound field reconstruction.

By referring to Table 2, the following conclusions can be drawn more clearly. It is discernible that the ACC-PM-L1 method and the ACC-PM-L2 method achieve a balance between AC and E_r in sound field control, ultimately resulting in highly effective sound field

control. At the same time, when compared to ACC-PM, these two methods have successfully reduced the filter order and the reproducing error in the bright zone sound field E_r, all while maintaining acoustic contrast AC.

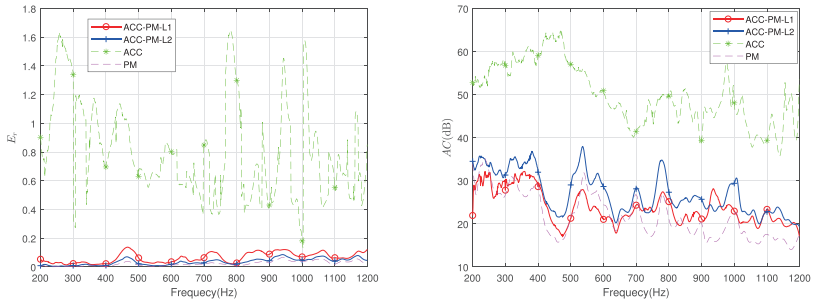

Figure 7: Comparison of E_r and AC with respect to frequency between the proposed methods and ACC, PM in numerical simulation.

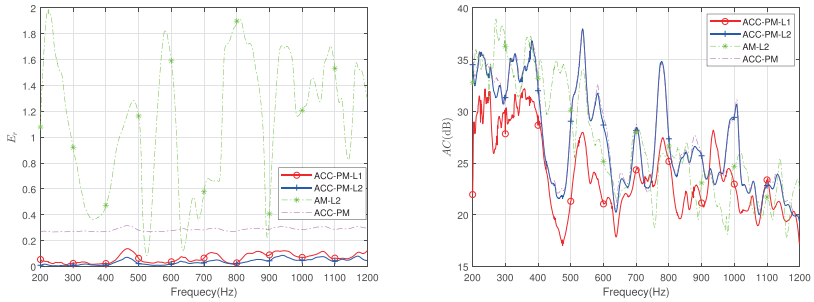

Figure 8: Comparison of E_r and AC with respect to frequency between the proposed methods and AM-L2, ACC-PM in numerical simulation.

4.3 Experiments using real data

In non-free field environments, phenomena like reflection, diffraction, and resonance in the spatial environment affect the transfer function, resulting in it containing more information. Consequently, it is impossible to fully validate the effectiveness of the sound field control model under simulated conditions.

To investigate the performance of the proposed methods in practical environment, we have conducted experiments using the impulse response dataset measured in the anechoic chamber experiment. The sound field is divided into left and right zones, and the layout of the laboratory is shown in Figure 9.

In our framework, the left row is designated as the bright zone Ω_B, and the right row is designated as the dark zone Ω_D. For the desired sound pressure, we set it to 1.0 in Ω_B and 0.0 in Ω_D, and the generated signal is a band-limited pulse signal ranging from 200 Hz to 1200 Hz. The interval between control frequency points $\triangle f$ is set to 1, and the sampling frequency f_s is 48kHz. The regularization parameter μ in Equation (2.3) for ACC and γ in Equation (2.5) for PM are both set as 1.0×10^{-5}. The penalty parameter in

Equation (4.1) for AM-L2 is set to 0.014. The parameter δ_1 and δ_2 are set to 13.9 and 0.21 in both Equation (ACC-PM-L1) and Equation (ACC-PM-L2). Meanwhile, in the control group ACC-PM, parameter δ is set as 13.9.

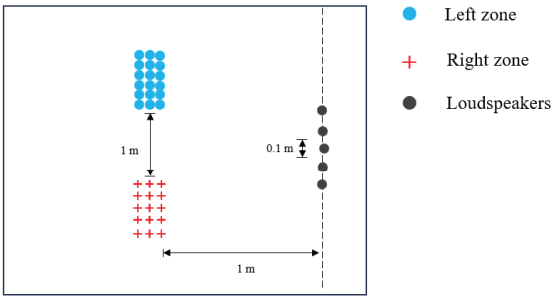

Figure 9: Loudspeakers position on the car roof.

Table 3: The optimal filters average order

	ACC-PM-L1	ACC-PM-L2	AM-L2	ACC-PM	ACC	PM
Order	6577	3296	2821	45412	45705	45021

As shown in Table 3, in non-free field scenarios, the AM-L2 method achieves the lowest filter order. However, as indicated by the subsequent results shown in Table 4, its sound field reproduction performance is not satisfactory. This also reflects the limitations of the AM method [13], which is more suitable for high-frequency situations where strict requirements on the phase of the sound field are not imposed. The ACC-PM-L2 method has the lower filter order, which is 3294, followed by the ACC-PM-L1 method, with an order of 6577. Compared to the other methods, it achieves a reduction of at least 30000 in filter order.

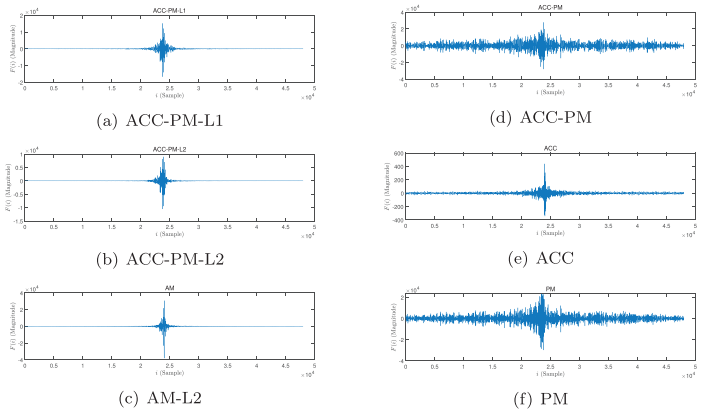

(a) ACC-PM-L1 (d) ACC-PM

(b) ACC-PM-L2 (e) ACC

(c) AM-L2 (f) PM

Figure 10: The 2th loudspeaker time-domain filters generated by using real data.

Figure 10 shows the FIR filters prior to truncation when using real data. In comparison

to the other three methods, the ACC-PM-L1 method and the ACC-PM-L2 method also display the most favorable truncation effect. Table 3 shows the optimal filters' average order of the loudspeaker-array for all methods, and the selection of optimal order for each filter is consistent with the simulation experiment.

From Figure 11, it is apparent that the oscillation level of the driving signal in real data is higher, contrary to findings from simulated data. This is due to the transfer function matrices of real data, which incorporate more environmental information. Therefore, it is necessary to use higher-order filters to accurately characterize the driving signal for effective sound field control.

Table 4: The average E_r and AC for all the frequency bins

	ACC-PM-L1	ACC-PM-L2	AM-L2	ACC-PM	ACC	PM
$\bar{AC}$	19.95	19.20	21.88	21.87	25.19	14.46
$\bar{E_r}$	0.22	0.25	0.99	0.17	0.50	0.13

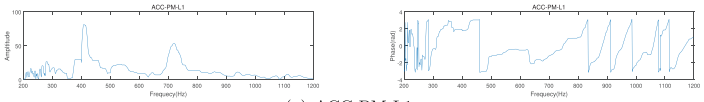

(a) ACC-PM-L1

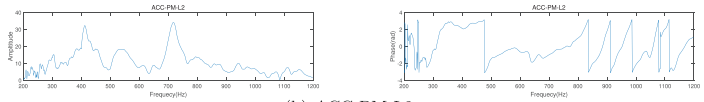

(b) ACC-PM-L2

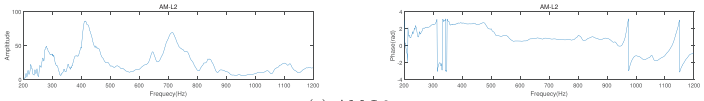

(c) AM-L2

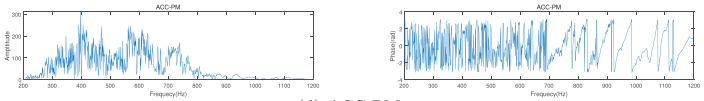

(d) ACC-PM

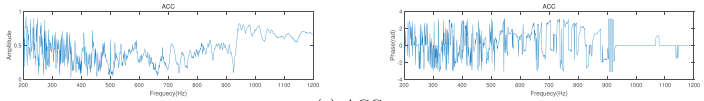

(e) ACC

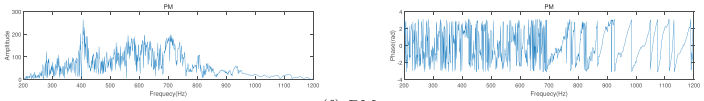

(f) PM

Figure 11: The 2th loudspeaker driving signal amplitude and phase by using real data.

Figure 12 illustrates the comparison between the methods proposed in this paper and ACC and PM methods in terms of metrics E_r and AC when using real data. Consistent with simulation results, the ACC-PM-L1 and ACC-PM-L2 methods achieve a balance between E_r and AC in sound field control, thereby effectively controlling the sound field. Figure 13 compares the methods proposed in this paper, ACC-PM, and AM-L2 methods. Compared to

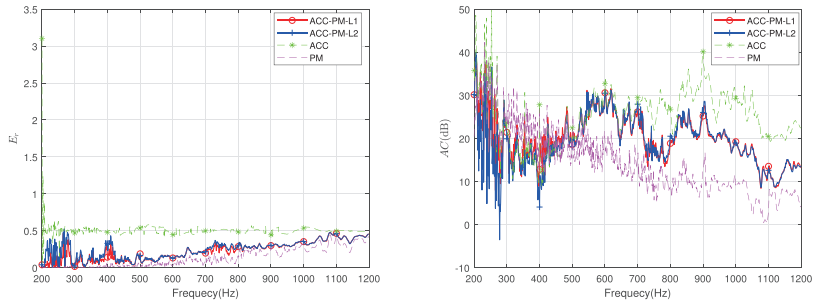

Figure 12: Comparison of E_r and AC with respect to frequency between the proposed methods and ACC, PM when using real data.

AM-L2, our proposed methods demonstrate superior accuracy in sound field reconstruction. Combined with Table 3 and Table 4, we conclude that the ACC-PM-L1 and ACC-PM-L2 methods achieve partitioned control of the sound field while significantly reducing filter order.

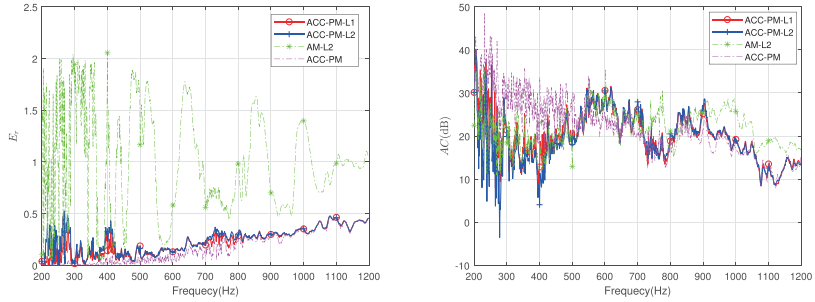

Figure 13: Comparison of E_r and AC with respect to frequency between the proposed methods and AM-L2, ACC-PM when using real data.

Comparison between simulated experiments and experiments using real data reveals different advantages of the ACC-PM-L1 and ACC-PM-L2 methods. In simulated experiments, the ACC-PM-L1 method shows better reduction in filter order, whereas in experiments using real data, the ACC-PM-L2 method exhibits better reduction in filter order. This variation arises due to differences in the properties of transfer function matrices between the two types of experiments.

5 Conclusion

This paper introduces two innovative methods, ACC-PM-L1 and ACC-PM-L2, for designing low-order filters in sound field control applications. The ACC-PM-L2 method utilizes a L2-norm based finite difference penalty (Diff.-L2 penalty) to achieve desired amplitude and phase synthesis while minimizing signal oscillations, thereby maintaining signal fidelity which is crucial for precise sound field control. The ACC-PM-L1 method incorporates a finite difference penalty based on the L1-norm (Diff.-L1 penalty) to enhance signal flatness by promoting sparsity in adjacent signal components. This effectively reduces filter complexity

while preserving essential signal characteristics and serves as a feature extraction method for broadband signals without significant fidelity loss. Numerical experiments demonstrate that both ACC-PM-L1 and ACC-PM-L2 methods effectively reduce filter orders compared to four benchmark methods in sound field control, while maintaining high performance levels. Considering the distinct properties of transfer function matrices, each of ACC-PM-L1 and ACC-PM-L2 offers unique advantages. Future research will investigate how these varying properties influence methods for partition control of sound fields, enhancing our understanding and applications of these methods in practical scenarios.

Acknowledgment

The authors would like to thank the two anonymous referees for their insightful comments and suggestions that have helped to improve the presentation of this paper greatly.

References

[1] T. Abe, S. Koyama, N. Ueno, et al., Amplitude matching for multizone sound field control, *IEEE Trans. Audio, Speech, Language Process* 31 (2022) 656–669.

[2] Y. Cai, Investigation on local sound reproduction using loudspeaker array, Chinese Academy of Science, Doctoral Thesis, 2014.

[3] Y. Cai, M. Wu, L. Liu, et al., Time-domain acoustic contrast control design with response differential constraint in personal audio systems, *J. Acoust. Soc. Am.* 135 (2014) 252–257.

[4] E. Candes and J. Romberg, L1-magic: Recovery of sparse signals via convex programming, URL: `https://candes.su.domains/software/l1magic/downloads/l1magic.pdf`, 2005.

[5] J.H. Chang and F. Jacobsen, Sound field control with a circular double-layer array of loudspeakers, *J. Acoust. Soc. Am.* 131 (2012) 4518–4525.

[6] J. Cheer, S. J. Elliott and M.F.S. Gálvez, Design and implementation of a car cabin personal audio system, *J. Audio Eng. Soc.* 61 (2013) 412–424.

[7] J.W. Choi and Y.H. Kim, Generation of an acoustically bright zone with an illuminated region using multiple sources, *J. Acoust. Soc. Am.* 111 (2002) 1695–700.

[8] P. Coleman, P.J.B. Jackson, M. Olik, et al., Acoustic contrast, planarity and robustness of sound zone methods using a circular loudspeaker array, *J. Acoust. Soc. Am.* 135 (2014) 1929–1940.

[9] S. Doclo and M. Moonen, GSVD-based optimal filtering for single and multimicrophone speech enhancement, *IEEE Trans. Signal Process.* 50 (2002) 2230–2244.

[10] W.F. Druyvesteyn and J. Garas, Personal sound, *J. Audio Eng. Soc.* 45 (1997) 685–701.

[11] S.J. Elliott and J. Cheer, Regularisation and robustness of personal audio systems, ISVR Technical Memorandum 995, University of Southampton, 2011.

[12] M. Hong and Z. Q. Luo, On the linear convergence of the alternating direction method of multipliers, *Math. Program.* 162 (2017) 165–199.

[13] S. Koyama, T. Amakasu, N. Ueno, et al., Amplitude matching: Majorization-minimization algorithm for sound field control only with amplitude constraint, in: *Proc. IEEE Int. Conf. Acoust., Speech, Signal Process* (ICASSP), 2021, pp. 411–415.

[14] L. Li, L. Wang, G. Wang, et al., Linearized alternating direction method of multipliers for separable convex optimization of real functions in complex domain, *J. Appl. Anal. Comput.* 9 (2019) 1686–1705.

[15] X. Liao, Personal sound control in a car cabin and research on accelerating sound quality, Tsinghua University, Doctoral Thesis, 2017.

[16] H. Luo and Z. Zhang, A unified differential equation solver approach for separable convex optimization: Splitting, acceleration and nonergodic rate, Math. Comp. (2025) https://doi.org/10.1090/mcom/4063.

[17] D. Needell, Noisy signal recovery via iterative reweighted L1-minimization, in: *2009 Conference Record of the Forty-Third Asilomar Conference on Signals, Systems and Computers*, IEEE, 2009, pp. 113–117.

[18] F. Olivieri, F.M. Fazi, P.A. Nelson, et al., Comparison of strategies for accurate reproduction of a target signal with compact arrays of loudspeakers for the generation of zones of private sound and silence, *J. Audio Eng. Soc.* 64 (2016) 905–917.

[19] J.B. Rosen, H. Park and J. Glick, Signal identification using a least L1 norm algorithm, *Optim. Eng.* 1 (2000) 51–65.

[20] D. Wallace, Practical Audio System Design for Private Speech Reproduction, University of Southampton, Doctoral Thesis, 2020.

[21] Y. J. Wu and T. D. Abhayapala, Spatial multizone soundfield reproduction: Theory and design, *IEEE Trans. Audio, Speech, Language Process* 19 (2010) 1711–1720.

A Appendix

A.1 Wirtinger's Derivatives

The signal preprocessing problem in sound field control system is actually the optimization of real functions in complex domain. The application of Wirtinger's Derivatives is necessary to find the optimal solution to this optimization problem.

Definition A.1 ([14])**.** Let $f : \mathbb{C} \to \mathbb{R}$ be a real-valued function over the complex domain. The Wirtinger's derivative of f at $\mathbf{z} = \mathbf{u} + i\mathbf{v}$ is defined as follows

$$\frac{\partial f}{\partial \mathbf{z}} := \frac{1}{2}\left(\frac{\partial f}{\partial \mathbf{u}} - i\frac{\partial f}{\partial \mathbf{v}}\right), \tag{A.1}$$

where $\frac{\partial f}{\partial u}$ and $\frac{\partial f}{\partial v}$ are the usual partial derivatives of f with respect to u and v. Moreover, the conjugate Wirtinger's derivative of f at $z = u + iv$ is defined as follows

$$\frac{\partial f}{\partial \bar{\mathbf{z}}} := \frac{1}{2}\left(\frac{\partial f}{\partial \mathbf{u}} + i\frac{\partial f}{\partial \mathbf{v}}\right).$$

Based on the above definition, we present the following example, which will be used in the subsequent analysis. Consider the quadratic function

$$f(z) = \|\boldsymbol{A}\mathbf{z} - \mathbf{b}\|^2, \quad \mathbf{z} \in \mathbb{C}, \tag{A.2}$$

where $\mathbf{b} \in \mathbf{C}^p$ and $\boldsymbol{A} \in \mathbf{C}^{p\times n}$. It holds that

$$\frac{\partial f}{\partial \mathbf{z}} = \boldsymbol{A}^T(\overline{\boldsymbol{A}\mathbf{z} - \mathbf{b}}), \quad \frac{\partial f}{\partial \bar{\mathbf{z}}} = \boldsymbol{A}^H(\boldsymbol{A}\mathbf{z} - \mathbf{b}).$$

If $\mathbf{z}^*$ is an extreme point of f, then it holds that $\frac{\partial f}{\partial \bar{\mathbf{z}}}(\mathbf{z}^*) = 0$.Therefore, the minimizer $\mathbf{z}^*$ of the quadratic function Equation (A.2) satisfies

$$\boldsymbol{A}^H(\boldsymbol{A}\mathbf{z}^* - \mathbf{b}) = 0.$$

A.2 Derivation of Equation (3.7)

The update rule for $\mathbf{q}$ is obtained by solving

$$\begin{aligned}
\mathbf{q}^{k+1} = \underset{\mathbf{q}\in\mathbb{C}^{JL}}{\operatorname{argmin}} \quad & \mathcal{L}_\rho(\mathbf{q}, \mathbf{z}^k; \boldsymbol{\mu}^k) \\
= \underset{\mathbf{q}\in\mathbb{C}^{JL}}{\operatorname{argmin}} \quad & \Big\{\| \boldsymbol{G}_{\mathrm{B}}\mathbf{q} - \mathbf{p}_{\mathrm{BT}}\|^2 + \delta_1\| \boldsymbol{G}_{\mathrm{D}}\mathbf{q}\|^2 \\
& + \mathrm{Re}((\boldsymbol{\mu}^k)^H(\boldsymbol{F}\mathbf{q} - \mathbf{z}^k)) + \frac{\rho}{2}\|\boldsymbol{F}\mathbf{q} - \mathbf{z}^k\|^2\Big\} \\
= \underset{\mathbf{q}\in\mathbb{C}^{JL}}{\operatorname{argmin}} \quad & \left\{\|\boldsymbol{G}_{\mathrm{B}}\mathbf{q} - \mathbf{p}_{\mathrm{BT}}\|^2 + \delta_1\|\boldsymbol{G}_{\mathrm{D}}\mathbf{q}\|^2 + \frac{\rho}{2}\left\|\boldsymbol{F}\mathbf{q} - \mathbf{z}^k + \frac{\boldsymbol{\mu}^k}{\rho}\right\|^2\right\}.
\end{aligned} \tag{A.3}$$

The optimal solution to the optimization problem Equation (A.3) can be obtained based on the definition and example provided in Appendix A.1. The update rule for $\mathbf{q}^{k+1}$ is:

$$\mathbf{q}^{k+1} = (\boldsymbol{G}_{\mathrm{B}}^H\boldsymbol{G}_{\mathrm{B}} + \delta_1\boldsymbol{G}_{\mathrm{D}}^H\boldsymbol{G}_{\mathrm{D}} + \delta_2\boldsymbol{F}^H\boldsymbol{F})^{-1}\left(\boldsymbol{G}_{\mathrm{B}}^H\mathbf{p}_{\mathrm{BT}} + \frac{\rho}{2}\boldsymbol{F}^H\mathbf{z}^k - \frac{1}{2}\boldsymbol{F}^H\boldsymbol{\mu}^k\right). \tag{A.4}$$

Similarly, the update rule for $\mathbf{z}$ is obtained by solving

$$\begin{aligned}
\mathbf{z}^{k+1} = \underset{\mathbf{z}\in\mathbb{C}^{(J-1)L}}{\operatorname{argmin}} \quad & \mathcal{L}_\rho(\mathbf{q}^{\mathbf{k+1}}, \mathbf{z}; \boldsymbol{\mu}^k) \\
= \underset{\mathbf{z}\in\mathbb{C}^{(J-1)L}}{\operatorname{argmin}} \quad & \left\{\delta_2\|\mathbf{z}\|_1 + Re\ ((\boldsymbol{\mu}^k)^H(\boldsymbol{F}\mathbf{q}^{k+1} - \mathbf{z})) + \frac{\rho}{2}\|\boldsymbol{F}\mathbf{q}^{k+1} - \mathbf{z}\|^2\right\} \\
= \underset{\mathbf{z}\in\mathbb{C}^{(J-1)L}}{\operatorname{argmin}} \quad & \left\{\|\mathbf{z}\|_1 + \frac{\rho}{2\delta_2}\left\|\boldsymbol{F}\mathbf{q}^{k+1} - \mathbf{z} + \frac{\boldsymbol{\mu}^k}{\rho}\right\|^2\right\} \\
= \underset{\mathbf{z}\in\mathbb{C}^{(J-1)L}}{\operatorname{argmin}} \quad & \left\{\|\operatorname{Re}(\mathbf{z})\|_1 + \frac{\rho}{2\delta_2}\left\|\operatorname{Re}(\mathbf{z}) - \operatorname{Re}\left(\boldsymbol{F}\mathbf{q}^{k+1} + \frac{\boldsymbol{\mu}^k}{\rho}\right)\right\|^2\right. \\
& \left. + i\|\operatorname{Im}(\mathbf{z})\|_1 + \frac{\rho}{2\delta_2}\left\|\operatorname{Im}(\mathbf{z}) - \operatorname{Im}\left(\boldsymbol{F}\mathbf{q}^{k+1} + \frac{\boldsymbol{\mu}^k}{\rho}\right)\right\|^2\right\} \\
= \mathbf{prox}_{t\|\cdot\|_1} \quad & \left(\operatorname{Re}\left(\boldsymbol{F}\mathbf{q}^{k+1} + \frac{\boldsymbol{\mu}^k}{\rho}\right)\right) + i\,\mathbf{prox}_{t\|\cdot\|_1}\left(\operatorname{Im}\left(\boldsymbol{F}\mathbf{q}^{k+1} + \frac{\boldsymbol{\mu}^k}{\rho}\right)\right),
\end{aligned}$$

where $t = \delta_2/\rho$.

Manuscript received 18 August 2023
revised 3 March 2024
accepted for publication 6 May 2024

Shu Tan
National Center for Applied Mathematics in Chongqing
Chongqing Normal University, Chongqing 401331, China
E-mail address: tanshu07@163.com

Hao Luo
National Center for Applied Mathematics in Chongqing
Chongqing Normal University, Chongqing 401331, China
E-mail address: luohao@cqnu.edu.cn

Xiangning Liao
Chongqing Changan Automobile Company Limited
Chongqing 400023, China
E-mail address: liaoxn@changan.com.cn

Fusheng Bai
National Center for Applied Mathematics in Chongqing
Chongqing Normal University, Chongqing 401331, China
E-mail address: fsbai@cqnu.edu.cn

Jie Li
Chongqing Changan Automobile Company Limited
Chongqing 400023, China
E-mail address: leejay1986@changan.com.cn